Herzschr Elektrophys 11:159–173 (2000)

N. Wessel
A. Voss
H. Malberg
C. Ziehmann
H.U. Voss
A. Schirdewan
U. Meyerfeldt
J. Kurths

Nonlinear analysis of complex phenomena in cardiological data

Received: 6 April 2000
Accepted: 26 July 2000

Dr. Niels Wessel (✉) · Christine Ziehmann
Jürgen Kurths
Nonlinear Dynamics Group
at the Institute of Physics
University of Potsdam
Am Neuen Palais 10
PF 601553
14415 Potsdam, Germany

Andreas Voss
University of Applied Sciences Jena
Germany

Hagen Malberg
University of Karlsruhe, Germany

Henning U. Voss
University of Freiburg, Germany

Alexander Schirdewan · Udo Meyerfeldt
Franz-Volhard-Hospital Berlin, Germany

Nichtlineare Analyse komplexer Phänomene in kardiologischen Datenreihen

Zusammenfassung Das Hauptanliegen dieses Beitrages ist es, verschiedene Ansätze in der Herzfrequenz- und Blutdruckvariabilität zu diskutieren und damit das Verständnis der kardiovaskulären Regulation zu verbessern. Wir betrachten Komplexitätsmaße basierend auf der symbolischen Dynamik, die renormierte Entropie und die ‚finite-time' Wachstumsraten. Weiterhin werden die duale Sequenzmethode zur Bestimmung der Baroreflexsensitivität sowie die Maximalkorrelationsmethode zur Schätzung der nichtlinearen Kopplung in bivariaten Daten vorgestellt. Letztere stellt eine geeignete Methode zur Bestimmung der Kopplungsstärke und –richtung dar. Herzfrequenz- und Blutdruckvariabilitätsdaten einer klinischen Pilotstudie und einer großangelegten klinischen Studie werden analysiert. Wir demonstrieren in diesem Beitrag, dass Methoden der nichtlinearen Dynamik nützlich sind für die Risikostratifizierung nach Herzinfarkt, für die Vorhersage von lebensbedrohlichen Rhythmusstörungen sowie für die Modellierung der Herzfrequenz- und Blutdruckregulation. Diese Ergebnisse könnten in der klinischen Diagnostik sowie für therapeutische und präventive Zwecke von implantierbaren Defibrillatoren der nächsten Generation von Bedeutung sein.

Schlüsselwörter Herzfrequenzvariabilität – Blutdruckvariabilität – Baroreflex – nichtlineare Kopplung – nichtlineare Dynamik – implantierbarer Defibrillator

Summary The main intention of this contribution is to discuss different nonlinear approaches to heart rate and blood pressure variability analysis for a better understanding of the cardiovascular regulation. We investigate measures of complexity which are based on symbolic dynamics, renormalised entropy and the finite time growth rates. The dual sequence method to estimate the baroreflex sensitivity and the maximal correlation method to estimate the nonlinear coupling between time series are employed for analysing bivariate data. The latter appears to be a suitable method to estimate the strength of the nonlinear coupling and the coupling direction. Heart rate and blood pressure data from clinical pilot studies and from very large clinical studies are analysed. We demonstrate that parameters from nonlinear dynamics are useful for risk stratification after myocardial infarction, for the prediction of life-threatening cardiac events even in short time series,

and for modelling the relationship between heart rate and blood pressure regulation. These findings could be of importance for clinical diagnostics, in algorithms for risk stratification, and for therapeutic and preventive tools of next generation implantable cardioverter defibrillators.

Key words Heart rate variability – blood pressure variability – baroreflex – nonlinear coupling – nonlinear dynamics – implantable defibrillator

Introduction

Annually, in the United States approximately 400 000 people die due to sudden cardiac death (4, 11). Therefore, an accurate and reliable identification of patients who are at high risk of sudden cardiac death is an important and challenging problem. Heart rate variability (HRV) parameters, calculated from the time series of the beat-to-beat-intervals, have been used to predict the mortality risk in patients with structural heart diseases (26, 57). We have recently demonstrated that a multivariate approach with HRV parameters including nonlinear methods as well as the combination of HRV measures with clinical parameters like the ejection fraction, the complexity of ventricular arrhythmias or the signal-averaged electrocardiogram significantly improves the results of risk stratification (59).

Physiological data very often show complex structures which cannot be interpreted immediately. The data we are analysing here are mainly heart rate and blood pressure variability (BPV) time series. Our main intention in this contribution is to discuss different approaches to obtain a better understanding of the underlying processes. In former studies on the one hand linear data analysis, especially correlation and spectral analysis (21), and on the other hand well-known nonlinear parameters, like correlation dimension or Lyapunov exponents, were used (2, 3, 17, 18, 27, 33). Among the variety of nonlinear approaches there are only a few studies which assess the clinical usefulness of nonlinear measures for high risk stratification based on heart rate or blood pressure variability analysis (25, 32, 35, 59, 60). No extensive prospective study has been performed to show the efficacy of these methods.

The disadvantage of the linear parameters is the limited information about the underlying complex system, whereas the nonlinear description suffers from the curse of dimensionality. Mostly, there are not enough points in the (often non-stationary) time series to reliably estimate these nonlinear measures. Therefore, we favour the measures of complexity which characterise quantitatively the dynamics even in rather short time series (30, 59, 60, 68). The measures of complexity we are using in this paper are based on symbolic dynamics, renormalised entropy and the finite time growth rates. Another main point in this contribution are methods to analyse bivariate data. We describe the dual sequence method to estimate the baroreflex sensitivity and the maximal correlation method to measure the coupling between time series. A further interesting field are synchronous effects like cardiorespiratory control (24, 52). The application of new sophisticated synchronisation methods (23, 50, 52, 55) seems to be very promising to the heart rate and blood pressure variability data sets, but this is beyond the scope of this paper.

The analysis of heart rate or blood pressure variability (BPV) is often difficult due to excessive artefacts and arrhythmias. While occasional ectopic beats are treated successfully by most preprocessing methods, more complex arrhythmias or arrhythmias which are similar to normal HRV fluctuations may remain untreated. Therefore, preprocessing of the data is presented comprehensively.

The paper is organised as follows. In the Data processing section we describe the preprocessing procedure. In section Methods we present parameters from nonlinear data analysis based on symbolic dynamics, renormalised entropy and finite-time growth rates. Additionally, the dual sequence analysis of the spontaneous baroreflex and the concept of maximal correlation are introduced, followed by the results of the data analyses and a discussion of our results.

Data preprocessing

The main objective in the analysis of heart rate and blood pressure is to investigate the behaviour of the cardiovascular system. Therefore, it is necessary to exclude not only artefacts (e.g. double recognition, i.e. R-peak and T-wave recognised as two beats) but also beats not coming from the sinus node of the heart (ventricular premature complexes – VPC). VPCs are not controlled by the autonomous nervous system and, thus, they are not part of the autonomous regulation. Practically, this exclusion means a filtering of the time series. In this paper the original time series are denoted as the RR-series (derived from the RR-intervals) and the filtered time series as NN-series (normal-to-normal-beat-interval).

VPCs in the tachogram are usually characterised by a very short interval followed by a very long RR-interval (ventricular premature beat) or, respectively, only by a very short interval (superventricular premature beat). The 20% filter (19, 26, 72) considers these facts; if the current value of the tachogram differs more than 20% from its predecessor the current value and its successor are marked as not normal. The advantage of this filter is the very simple rule; however, the disadvantages are

rarely considered. VPCs with less than 20% difference are not removed from the series and may falsify almost all HRV or BPV parameters. The RR-intervals recognised as not normal are treated in different ways: either they are simply removed from the series or linear or spline interpolated (5, 31). The disadvantage of simply removing the beats is the loss of time dependence. Interpolating linearly may lead to false decreased variabilities, interpolating with splines often fails in time series with many VPCs.

In the following a new adaptive filtering algorithm is presented which is based on the idea of the interval filter described in Wessel et al. (67). The new filtering algorithm consists of three sub-procedures: (i) the removal of obvious recognition errors, (ii) the adaptive percent-filter, and (iii) the adaptive controlling filter.

- Obvious misrecognitions are RR-intervals of length zero, beat-to-beat intervals less than 200 ms (human refractory time) and pauses, i.e. when the heart does not pump for a certain time. These pauses were evaluated with every clinical Holter system; therefore, we do not consider them.
- The adaptive filtering procedure was developed based on the adaptive mean value μ_a and the adaptive standard deviation σ_a. Firstly, to estimate the basic variability in the series a binomial-7-filtered series is calculated. Given the tachogram x_1, $x_2,\ldots,$ x_N, the binomial filtered series is given by

$$t_n = \frac{x_{n-3} + 6x_{n-2} + 15x_{n-1} + 20x_n + 15x_{n+1} + 6x_{n+2} + x_{n+3}}{64} \quad (1)$$

The filtered series $t_1, t_2, \ldots, t_N$ reflects the global behaviour of sinus node activity without the influence of artefacts and VPCs. The adaptive mean value μ_a and the adaptive standard deviation σ_a of the binomial filtered series $t_1, t_2, \ldots, t_N$ are defined as:

$$\mu_a(n) := \mu_a(n-1) - c(\mu_a(n-1) - t_{n-1}) \quad (2)$$

$$\sigma_a(n) := \sqrt{\mu_a(n)^2 - \lambda_a(n)} \quad (3)$$

where c is a controlling coefficient $c \in [0,1]$ and $\lambda_a(n)$ is the adaptive second moment

$$\lambda_a(n) := \lambda_a(n-1) - c(\lambda_a(n-1) - t_{n-1} \cdot t_{n-1}) \quad (4)$$

The exclusion rule of this filter reads as follows: the RR-interval x_n is classified as not normal, if

$$|x_n - x_{n-1}| > \frac{p}{100} x_{n-1} + c_f \cdot \bar{\sigma}_a \quad \text{and} \quad |x_n - x_{lv}| > \frac{p}{100} x_{lv} + c_f \cdot \bar{\sigma}_a \quad (5)$$

where p is a proportional limit (here 10%), $c_f \cdot \bar{\sigma}_a$ is a generalised 3σ-rule, x_{lv} is the last valid RR-interval and $\bar{\sigma}_a$ is the averaged σ_a. Values recognised as not normal are replaced with a random number from $[\mu_a(n) - \frac{1}{2}\sigma_a(n), \mu_a(n) + \frac{1}{2}\sigma_a(n)]$ to avoid false decreased variabilities.

- Finally, as a precaution, the adaptive controlling procedure follows. From the resulting time series $x_1^{\%}, x_2^{\%}, x_3^{\%}, \ldots$ of the adaptive percent-filter, the binomial filtered series and the respective adaptive mean value and standard deviation are again calculated. The value $x_n^{\%}$ is considered to be not normal if

$$\left|x_n^{\%} - \mu_a(n)\right| > c_{f_1} \cdot \sigma_a(n) + \sigma_b \,, \quad (6)$$

where c_{f_1} is the filter coefficient (here $c_{f_1} = 3.0$) and σ_b stands for a basic variability (for HRV here $\sigma_b = 20$ ms). This basic variability σ_b was introduced to reduce filtering errors for time series with low variability (near the accuracy of RR-interval detection). Not normal values are replaced with the respective values of the binomial filtered series.

The advantage of this adaptive filtering procedure is the spontaneous adaptation of the filter coefficients due to sudden changes in the series (e.g. sudden heart rate increase).

Methods

In this section methods of nonlinear data analysis are presented. The subsections A–C refer to univariate data records, whereas D and E are about bivariate data analysis.

Symbolic dynamics

Symbolic dynamics was introduced, as far as we know, as early as Hadamard's (20) ideas to analyse complicated systems in 1898. An important point of this work was a simple description of the possible sequences that can arise in geodesic flows on surfaces of negative curvature. He introduced a finite set of forbidden symbol pairs and defined possible sequences as those that do not contain any forbidden symbol pair. Later on, Hedlund and Morse (40, 41) used this method to prove the existence of periodic and other dynamics in different classical dynamical systems. They showed that in many circumstances a finite description of a system's dynamics is possible. Symbolic dynamics today represents a rapidly growing and essential part of dynamical systems analysis and its application to physiology (7, 8, 14, 30, 60, 44, 47, 48, 70).

Heart rate and blood pressure variability reflect the complex interactions of many different control loops of the cardiovascular system. In relation to the complexity of the sinus node activity modulation system, a more predominantly nonlinear behaviour has to be assumed. Thus, the detailed description and

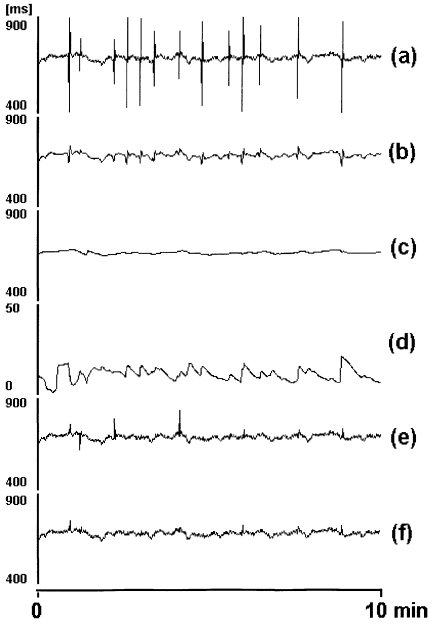

Fig. 1 The procedure of data preprocessing. From the original time series (**a**) a binomial filtered time series (**b**) is calculated to estimate the basic variability (compare Eq. (1)). From the filtered time series (**b**) the adaptive mean value (**c**) and the adaptive standard deviation (**d**) are estimated to quantify local changes in variability (compare Eqs. (2) and (3)). With the exclusion rule given in Eq. (5) based on proportional deviations from predecessors many VPCs and artefacts can be removed from the original time series (**e**). Finally, using the adaptive controlling procedure from Eq. (6) almost all remaining disturbances can be eliminated (**f**)

Abb. 1 Die Datenvorverarbeitung. Von der originalen Zeitreihe (**a**) wird eine binomialgefilterte Reihe (**b**) zur Bestimmung der Grundvariabilität berechnet (vgl. Formel (1)). Von der gefilterten Zeitreihe (**b**) wird der adaptive Mittelwert (**c**) und die adaptive Standardabweichung (**d**) zur Quantifizierung von lokalen Variabilitätsveränderungen bestimmt (vgl. Formeln (2) und (3)). Mit der Ausschlussregel, welche in Formel (5) gegeben ist und welche auf prozentualen Abweichungen vom Vorgänger basiert, können viele Extrasystolen und Artefakte beseitigt werden (**e**). Abschließend, unter Benutzung des adaptiven Kontrollfilters aus Formel (6) können nahezu alle restlichen Störungen beseitigt werden (**f**)

classification of dynamic changes using time and frequency measures is often not sufficient. Therefore, we have introduced new methods of nonlinear dynamics derived from the symbolic dynamics to distinguish between different states of the autonomic interactions (30, 60). The first step of this approach is the transformation of the time series into symbol sequences with symbols from a given alphabet. Some detailed information is lost in this process, but the coarse dynamic behaviour can be analysed. Wackerbauer et al. (65) used the methodology of symbolic dynamics for the analysis of the logistic map where a generic partition is known. However, for physiological time series analysis a more pragmatic approach is necessary. The transformations into symbols have to be chosen on a context-dependent basis. For this reason, we developed measures of complexity on the basis of such context-dependent transformations, which have a close connection to physiological phenomena and are relatively easy to interpret.

Comparing different kinds of symbol transformations, we found that the use of four symbols, as explained in Eq. (7), was appropriate for our purpose.

The time series $x_1, x_2, x_3, \ldots, x_N$ is transformed into the symbol sequence $s_1, s_2, s_3, \ldots, s_N$, $s_i \in A$ on the basis of the alphabet $A = \{0,1,2,3\}$. The transformation into symbols refers to three given levels where μ denotes the mean beat-to-beat interval and a is a special parameter that we have chosen 0.05; we tested several values of a from 0.05 to 0.08, but the resulting symbol sequences did not significantly differ (see Fig. 2),

$$s_i(x_i) = \begin{cases} 0: & \mu & < x_i \leq & (1+a)\mu \\ 1: & (1+a)\mu & < x_i < & \infty \\ 2: & (1-a)\mu & < x_i \leq & \mu \\ 3: & 0 & < x_i \leq & (1-a)\mu \end{cases} \quad \text{where } i = 1, 2, 3, \ldots \tag{7}$$

There are several quantities that characterise such symbol strings. We analyse the frequency distribution of words of length 3, i.e. substrings which consist of three adjacent symbols leading to a maximum 64 different words (bins). This is a compromise between retaining important dynamical information and of having robust statistics to estimate the probability distribution (compare Fig. 2).

We consider 3 measures of complexity:

- The Shannon entropy H_k calculated from the distribution p of words is the classic measure for the complexity in time series:

$$H_k = -\sum_{\omega \in W^k, p(\omega) > 0} p(\omega) \log p(\omega) \tag{8}$$

where W^k is the set of all words of length k. Larger values of Shannon entropy refer to higher complexity in the corresponding tachograms and lower values to lower ones.
- 'Forbidden words' in the distribution of words of length 3 are the number of words which never (or almost never) occur. A high number of forbidden words reflects a rather regular behaviour in the time series. If the time series is highly complex in the Shannonian sense, only a few forbidden words are found.
- The parameter 'plvar10' characterising short phases of low variability from successive symbols of another simplified alphabet B, consisting only of symbols '0' and '1'. Here '0' stands for a small difference between two successive RR-intervals (the resolution of the defibrillators used in this study), whereas '1' represents cases when the difference between two successive RR-intervals exceeds a certain limit, specifically

$$s_n = \begin{cases} 1: & |x_n - x_{n-1}| \geq 10 \text{ ms} \\ 0: & |x_n - x_{n-1}| < 10 \text{ ms} \end{cases} \tag{9}$$

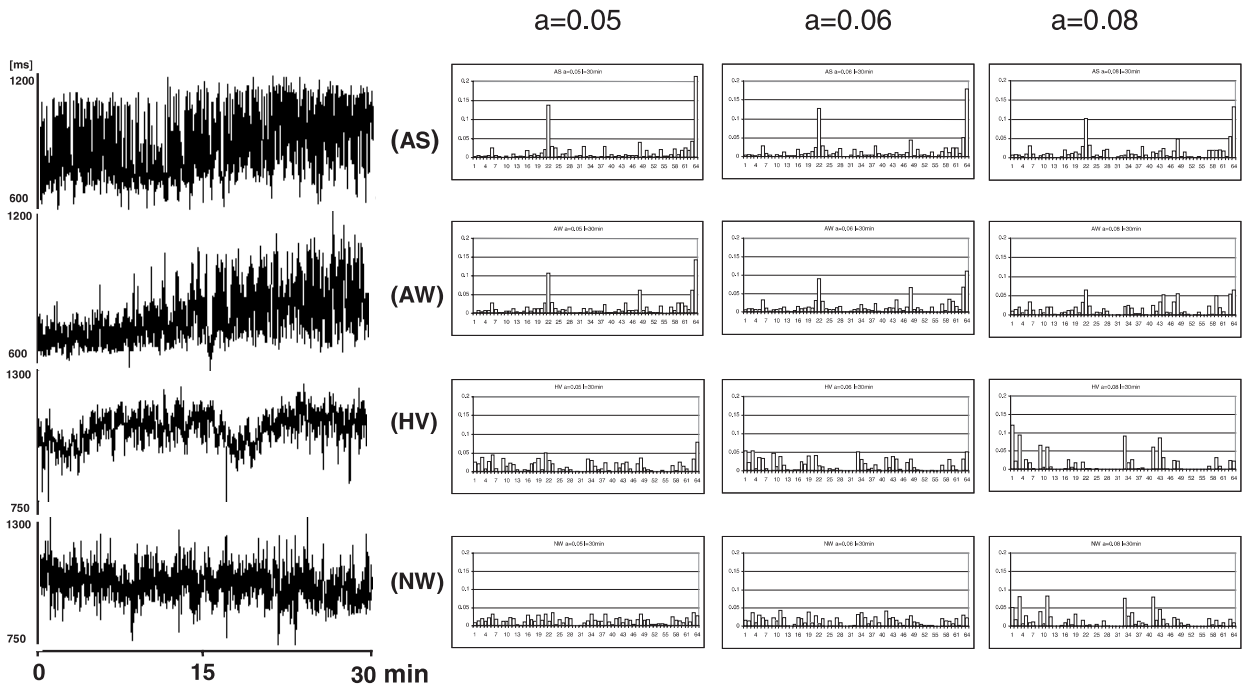

Fig. 2 Symbolic dynamics – the dependence on controlling parameter *a* (see Eq. 7). On the left side the original tachograms (notations AS, AW, HV, NW) are presented followed by the respective word distributions for controlling parameters *a* equal to 0.05, 0.06 and 0.08

Abb. 2 Symbolische Dynamik – die Abhängigkeit vom Kontrollparameter *a* (vgl. Formel 7). Links sind die Originaltachogramme (Bezeichnungen AS, AW, HV, NW) dargestellt, gefolgt von den dazugehörigen Wortverteilungen für den Parameter *a* gleich 0,05, 0,06 und 0,08

Words consisting of unique types of symbols (either all '0' or all '1') were counted. To obtain a statistically robust estimate of the word distribution, we chose words of length six, defining a maximum of 64 different words. 'Plvar10' represents the probability of the word '000000' occurrence and thus detects even intermittently decreased HRV.

Renormalised entropy

Another nonlinear method which might be capable of assessing complex properties of cardiac periodograms is the 'renormalised entropy.' The basic idea is to determine the complexity of cardiac periodograms based on a fixed reference. Based on general considerations in thermodynamics, Klimontovich suggested comparing the relative degree of order of two different distributions by renormalising the reference distribution to a given energy. Saparin (51) proposed a procedure for calculating this quantity from time series and applied it to the logistic map. Applications of renormalised entropy to physiological data were previously introduced (28, 30, 60, 67). As the application to heart rate data method suffers from potential lack of reproducibility, another method for the computation of renormalised entropy $\mathrm{RE}_{\mathrm{AR}}$ based on an autoregressive spectral estimation has been recently developed (66).

To compare the relative degree of order of two different distributions, the reference distribution is renormalised to a given energy. The complexity of any distribution in relation to a fixed reference distribution is estimated by solving an integral equation. Considering two tachograms (time series of beat-to-beat intervals) with the density distribution estimates $f_0(x)$ and $f_1(x)$ and using the estimate $f_0(x)$ as a reference, the renormalised density distribution $\bar{f}_0(x)$ of $f_0(x)$ is defined as:

$$\bar{f}_0(x) := \frac{f_0(x)^T}{\int f_0(x)^T dx} \tag{10}$$

where T is the solution of the integral equation

$$\int \ln f_0(x)^{(\bar{f}_0(x)-f_1(x))} dx = 0 \tag{11}$$

The solution of Eq. (11) has to be determined numerically. The renormalised entropy RE of the distribution $f_1(x)$ is defined by the following interchanging algorithm, where $S(f(x))$ is the Shannon entropy of distribution $f(x)$, that is

$$S(f(x)) = -\int f(x) \cdot \ln f(x) dx \tag{12}$$

Procedure:

- Calculate $\Delta_1 = S(f_1(x)) - S(\bar{f}_0(x))$ with the distribution

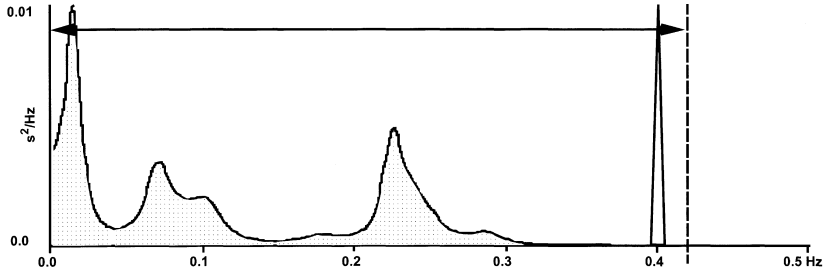

Fig. 3 The estimation of the tachogram distribution is the basis for calculating renormalised entropy. Here, the autoregressive spectral distribution (dotted) together with the calibration peak at 0.4 Hz was used. Given a fixed reference distribution, the complexity of all distributions which should be analysed will be determined relative to this reference

Abb. 3 Die Schätzung der Tachogrammverteilung dient als Grundlage zur Berechnung der renormierten Entropie. Hier wurde eine autoregressive Spektralschätzung (gepunktet) unter Einsatz eines Kalibrierungssignals bei 0,4 Hz benutzt. Ist eine Referenzverteilung festgelegt, so wird die Komplexität jeder zu untersuchenden Verteilung relativ zu dieser Referenz bestimmt

as the reference ($f_0(x)$ is renormalised). The value of T is denoted $T_1 = T$.

- Calculate $\Delta_2 = S(f_0(x)) - S(\bar{f}_1(x))$ with the distribution $f_1(x)$ as the reference ($f_1(x)$ is renormalised). The resulting T value is denoted $T_2 = T$.
- If $T_1 > T_2$, the distribution $f_0(x)$ is found to be the more disordered one (in the sense of renormalised entropy – i.s.r.e.) and the renormalised entropy RE is defined as $RE = \Delta_1$. Otherwise ($T_1 < T_2$) $f_1(x)$ is the more disordered distribution (i.s.r.e.) and the renormalised entropy is $RE = -\Delta_2$.

Calculation of the renormalised entropy requires estimating the tachogram distributions. Here we use an autoregressive spectral estimation of the filtered and interpolated tachogram. A known problem of autoregressive spectral estimations is the bias which might appear even in idealised circumstances. To overcome this problem a sinusoidal oscillation with a fixed amplitude and frequency was added to the time series. The amplitude of 40 ms was chosen to obtain a dominant peak in the spectral estimation, and the frequency was set to 0.4 Hz, which is the upper limit of the high frequency band (21) (compare Fig. 3). A spectral density estimation in the interval $[0, 0.42]$ Hz was used to include all physiological modulations, and the calibration peak. Using a reference tachogram from a healthy subject with normal low and high frequency modulations the RE_{AR} method is designed so that either a decreased HRV or a pathological spectrum leads to positive values of renormalised entropy.

Finite time growth rates

Lyapunov exponents of a dynamical system reflect effective growth rates of infinitesimal uncertainties over an infinite duration, yet, time series analysis is restricted to the analysis of finite time series and thus it is difficult to determine Lyapunov exponents reliably (13, 29, 43, 53, 69). Therefore, we concentrated on quantifying the state-dependent short-term predictability through finite-time growth rates. Note that these differ from the finite-time Lyapunov exponents (1, 10, 34, 71, 73) as well as the finite-time growth rates described in (42), both of which require the knowledge of the tangent maps thus the equations governing the dynamics. In Ziehmann et al. (73) the significant differences between these quantities are discussed.

Our finite-time growth rates are approximations based on the idea of Wolf et al. (69). Firstly, pseudo-phase spaces of the system are constructed using delay coordinates (54). Their dimension is denoted by n and the fixed delay by τ. Next, for each point in this constructed phase space $X_k = [x_{k+1\tau}, x_{k+2\tau}, \ldots, x_{k+(n-1)\tau}]$, $k = 0, \ldots, N-(n-1)\tau$ of the measured tachogram $X = [x_1, x_2, \ldots, x_N]$ the nearest neighbour $\bar{X}_k$ is determined. $\bar{X}_k$ is defined as that state which has the minimal Euclidean distance to X_k. $\|X_u - X_v\|$ denotes the Euclidean distance of the state X_u to X_v, i.e.

$$\|X_u - X_v\| = \sqrt{\sum_{j=1}^{n-1} (x_{u+j\tau} - x_{v+j\tau})^2} \qquad (13)$$

Then the minimal distance d_k to the I_k state is given by

$$\begin{aligned} d_k = \min & \\ & \{\|X_k - X_i\| \\ & |i = 0, \ldots, N-(n-1)\tau, \\ & |i-k| > (n-1)\tau\}, \\ & k = 0, \ldots, N-(n-1)\tau \end{aligned} \qquad (14)$$

and the nearest neighbour by

$$\begin{aligned} \bar{X}_k = \{X_m | \|X_k - X_m\| = d_k\}, \\ k = 0, \ldots, N-(n-1)\tau \end{aligned} \qquad (15)$$

Note that the time lag of the nearest neighbour has to be at least one window length, i.e. $|i-k| > (n-1)\tau$ and we only consider points as neighbours if their distance to the base point is less than 10% of the maximum distance between any two points. Next, we analyse the evolution of the states X_k and $\bar{X}_k$ during the time T. After these T steps we obtain the states $X_k^T = [x_{k+T+1\tau}, x_{k+T+2\tau}, \ldots, x_{k+T+(n-1)\tau}]$ and $\bar{X}_k^T$ respectively. The distance between both states $\|X_k^T - \bar{X}_k^T\|$ represents the divergence after T evolution steps. From the original distance of both states

and the distance after T steps we calculate the finite-time growth rate $\lambda_k^{(n,\tau,T)}$:

$$\lambda_k^{(n,\tau,T)} = \frac{1}{T}\ln\frac{\|X_k^T - \bar{X}_k^T\|}{\|X_k - X_k\|} \qquad (16)$$
$$k = 0,\ldots,N-(n-1)\tau$$

$\lambda_k^{(n,\tau,T)}$ quantifies the local short-term predictability at the point X_k. If these $\lambda_k^{(n,\tau,T)}$ are greater than zero, the distance after the evolution time increases; otherwise, it decreases.

We calculate the finite-time growth rates for each point of the delay phase space, which leads to a growth rate time series $\lambda_k^{(n,\tau,T)}$. Its average, the average growth rate $\lambda_k^{(n,\tau,T)}$,

$$\lambda_k^{(n.\tau,T)} = \frac{1}{N-(n-1)\tau+1} \times \sum_{k=0}^{N-(n-1)\tau} \lambda_k^{(n.\tau,T)} \qquad (17)$$

quantifies a global short-term predictability. The dimension n, i.e. the length of the selected tachogram, part varied from 3 to 9. We chose this range to cover an interval up to 9, which is a typical order of an autoregressive model for short-term HRV tachograms (67). The evolution time and the delay are defined as T=1,2,3 and τ=1,2,3 respectively.

Additionally, to reduce random influences, we consider a three and a five nearest neighbour approach. According to Eq. (15) we determine the five nearest neighbours $I_k^1,\ldots,I_k^5$ of the point I_k and evolve all neighbours over the evolution time T. The finite-time growth rates for the three and the five nearest neighbour approach are derived from the average distances before and after the evolution time.

Dual sequence method

The dual sequence method (DSM) (36, 37) was developed for the estimation of the spontaneous baroreflex sensitivity from the bivariate heart rate and blood pressure data. Two kinds of RR-interval (beat-to-beat interval) responses were analysed: bradycardic (blood pressure increase causes RR-interval increase) and tachycardic (blood pressure decrease causes RR-interval decrease) fluctuations, where primarily the bradycardic fluctuations represent the vagal spontaneous baroreflex (12, 39). The analysis of the tachycardic fluctuations allows the investigation of the relation between the vagally (bradycardic) and sympathetically (tachycardic) mediated fluctuations of heart rate.

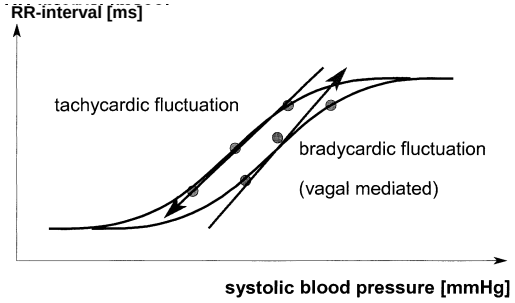

Fig. 4 The baroreflex regulatory behaviour: the points reflect the corresponding discrete systolic blood pressure and RR-intervals, the regression lines demonstrate the estimation of the real slopes (curves)

Abb. 4 Die Baroreflexregulation: die Punkte repräsentieren die entsprechenden diskreten systolischen Blutdruck- und RR-Intervall-Werte, die Regressionslinie demonstriert die Schätzung der realen Anstiege

Applying the DSM, the baroreflex sensitivity slopes were determined from three consecutive blood pressure and RR-interval values (see Fig. 4). Sequences of more than three values were proved not to be useful, because of the short duration of spontaneous heart rate and blood pressure fluctuations, in contrast to pharmacologically induced changes (46). The calculated slopes were grouped into defined slope classes. Additionally, the total number and the percentage to the total number of all slopes were calculated.

Former studies showed that the heart rate does not respond simultaneously to the blood pressure fluctuation. Obviously, the heart rate response depends on the different velocity of vagal and sympathetic regulation (38, 39). In contrast to other sequence methods (6, 45), the time series are shifted to register the synchronous and the postponed heart rate response on the same BP fluctuation.

The following parameter groups are calculated by DSM:

- The total number of slopes in the different sectors within the time series,
- The percentage of the slopes to the total number of slopes in the different sectors,
- The numbers of bradycardic and tachycardic slopes,
- The shift operation from the first to the third heart beat triple and
- The average slopes of all fluctuations.

These parameters are calculated for bradycardic as well as for tachycardic fluctuations up to a delay of 80 values to analyse the long-term and maximal response of the heart rate to the same blood pressure oscillation. Additionally, parameters from HRV and BPV analysis are calculated to investigate a possible common application to risk stratification.

Nonlinear regression and optimal transformations

Optimal transformations and the associated concept of maximal corre-

lation provide a nonparametric procedure to detect and determine nonlinear relationships in bivariate data sets. Let X and Y denote two zero-mean data sets and

$$R(X, Y) = \frac{E[XY]}{\sqrt{E[X^2]E[Y^2]}} \quad (18)$$

their (normalised) linear correlation coefficient, where $E[.]$ is the expectation value. The basic idea of this approach is to find such transformations $\Theta(Y)$ and $\Phi(X)$ that the absolute value of the correlation coefficient between the transformed variables is maximised. This leads to the *maximal correlation* (16, 22, 49).

$$\Psi(X, Y) := \sup_{\Theta,\Phi} |R(\Theta(Y), \Phi(X))| \quad (19)$$

The functions $\Theta(Y)$ and $\Phi(X)$ for which the supremum is attained are called *optimal transformations*. This concept generalises the linear correlation, where the linear correlation coefficient $R(X,Y)$ quantifies only linear dependencies

$$Y = aX + \eta \quad (20)$$

while $\Psi(X, Y)$ quantifies nonlinear dependencies of the form

$$\Theta(Y) = \Phi(X) + \eta \quad (21)$$

Especially, if there is complete statistical dependence (49), i.e. Y is a function of X or vice versa, the maximal correlation attains unity. This is also true for the relation (21) with $\eta = 0$. Here we are mainly interested in the estimation of the optimal transformations for the multivariate regression problem

$$\Theta(Y) = \Phi_1(X_1) + \ldots + \Phi_m(X_m) + \eta \quad (22)$$

This is an additive model for the (not necessarily independent) input variables $Y, X_1, \ldots, X_m$. The regression functions involved can be estimated as the optimal transformations for the multivariate problem analogous to Eq. (19). To estimate them nonparametrically, we use the *Alternating Conditional Expectation* (ACE) algorithm (9). This iterative procedure is nonparametric because the optimal transformations are estimated by local smoothing of the data using kernel estimators. We use a modified algorithm[1] in which the data are rank-ordered before the optimal transformations are estimated. This makes the result less sensitive to the data distribution. It should be mentioned that optimal transformations for multiplicative combinations of variables $\tilde{X}_1, \ldots, \tilde{X}_l$ can be estimated by forming

$$X_i = h_i(\tilde{X}_1, \ldots, \tilde{X}_l) \quad (23)$$

where the h_i are arbitrary functions.

The maximal correlation and optimal transformations have been applied to identify delay (61) and partial differential equations (63). In the application to differential equations, time derivatives have to be estimated from the data. The effect of noise on the estimated optimal transformations is not yet completely understood. On the one hand, for neglectable amounts of noise this approach has successfully been applied to experimental physical data of different origin (62, 64), yielding even quantitatively accurate results. On the other hand, if noise contamination is strong, this method should be used as an exploratory tool in the process of model selection. To minimise the influence of the noise on the results, the variable with the best signal-to-noise ratio, usually the undifferentiated time series, should be chosen as Y.

Table 1 The mean error of HRV parameters for two different filtering procedures (see text) and different superimposed signals

Tab. 1 Der mittlere Fehler der HRV-Parameter für zwei verschiedene Filterprozeduren (vgl. Text) und verschiedene überlagerte Signale

Mean error [%]	Adaptive filter	20% filter
VPC 100 ms premature	5.99	13.55
VPC 200 ms premature	5.27	18.68
VPC 300 ms premature	6.34	16.43
Trigemini 300 ms premature	8.10	57.89
Bigemini 300 ms premature	17.64	92.36

Results

Preprocessing

To test the accuracy of the filtering procedure, tachograms of normal healthy persons were superimposed by simulated ventricular premature complexes (VPC) of different kinds. Applicable preprocessing procedures should be able to remove these superimposed signals to obtain approximately the same series as before. Besides singular VPCs, several complexes of trigeminus and bigeminus were also superimposed. Next the HRV parameter from the time and frequency domain as well as from nonlinear dynamics were calculated. The parameter values of the original unfiltered time series were compared with the values of the filtered superimposed series. The mean error, given in Table 1, is calculated as the mean value of the relative errors of all parameters. The relative error is the deviation of the parameter calculated from the filtered to the original unfiltered parameter value. As one can see, even for trigeminus periods the adaptive filtering procedure seems to work reliably. On the contrary, the results of the 20% filter demonstrate that this filter is not sufficient for an accurate time series analysis. The

[1] A MATLAB – and a C-program for the ACE algorithm can be obtained from the authors or from the web page http://www.fdm.uni-freiburg.de/~hv/hv.html.

mean error of the adaptive filter increases rapidly for episodes of bigeminus – the filter should not be used in such cases. However, with this filtering procedure we obtain much better results; therefore, the adaptive filtering procedure is used here.

Symbolic dynamics in a large clinical study

In an extensive clinical study a multiparametric heart rate variability analysis was performed (59) to test if a combination of HRV measures improves the result of risk stratification in patients after myocardial infarction. Standard time domain, frequency domain and symbolic dynamics measures of HRV assessment were applied to 572 survivors of acute myocardial infarction. Of them 43 died in the follow-up time of two years. Besides some linear parameters almost all parameters from symbolic dynamics showed significant differences between the follow-up survivors and the deceased. A correlation analysis was performed (58) and showed that HRV analysis based on symbolic dynamics is an independent assessment and has only weak correlations with time (0.38 ± 0.13) and frequency (0.27 ± 0.14) domain parameters. Finally, for this population we could show that a multiparametric approach with the combination of four parameters from all domains is a better predictor of high arrhythmia risk than the standard measurement of global heart rate variability.

Renormalised entropy in a clinical pilot study

In a clinical pilot study the renormalised entropy RE_{AR} was applied to data of 18 cardiac patients and 23 healthy subjects. The cardiac patient group consisted of patients after myocardial infarction with documented life threatening ventricular arrhythmias; 10 of them were survivors of a sudden cardiac arrest who received automatic implantable defibrillators. From the group of healthy subjects, the most disordered tachogram (i.s.r.e.) was determined as the reference for RE_{AR} calculation ($RE_{AR} = 0$ for healthy person no. 16). Figure 5 shows the result of this clinical pilot study. Renormalised entropy RE_{AR} correctly classified 13 of 18 high risk patients (greater than zero or under the dashed line at –0.33). The previously introduced method (60) classified correctly only 7 high risk patients.

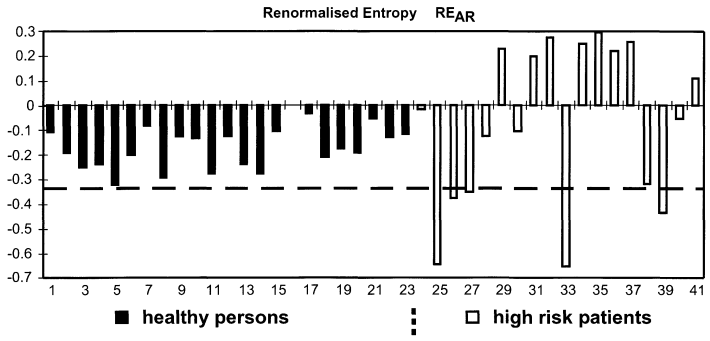

Fig. 5 Results of renormalised entropy in a clinical pilot study, black bars represent the control group whereas the white bars refer to the cardiac patients

Abb. 5 Die Ergebnisse der renormierten Entropie in der klinischen Pilotstudie, schwarze Balken repräsentieren die Kontrollgruppe, weiße die Herzpatienten

Finite-time growth rates and symbolic dynamics in forecasting cardiac arrhythmias

Recent studies showed that HRV assesses the autonomic nervous system dysfunction and is able to identify patients at risk of sudden cardiac death (15, 21); however, these methods were not developed to perform short-term predictions of malignant ventricular arrhythmias. The objective of this study was to find early signs of sustained ventricular tachycardia/ventricular fibrillation (VT/VF) in patients with an implanted cardioverter-defibrillator (ICD). These devices are able to safeguard patients by returning their hearts to a normal rhythm via strong defibrillatory shocks; additionally, they store the 1000 beat-to-beat intervals immediately before the onset of a life-threatening arrhythmia. We analysed these 1000 beat-to-beat intervals of 17 chronic heart failure ICD patients before the onset of a life-threatening arrhythmia and at a control time, i.e. without VT/VF event (68). To characterise these rather short data sets, we calculated heart rate variability parameters from time and frequency domain, from symbolic dynamics as well as the finite-time growth rates. We found that neither the time nor the frequency domain parameters show significant differences between the VT/VF and the control time series. As already visible in Fig. 6, only the mean beat-to-beat interval showed a remarkable but nonsignificant difference between the groups.

Two parameters from symbolic dynamics, however, as well as the finite-time growth rates significantly discriminate both groups (see Table 2). The Shannon entropy of the word distribution H_k is significantly higher in the control group, whereas the low-variability measure 'plvar10' is larger in the VT/VF group. Both parameters indicate a partly decreased heart rate variability in the VT/VF group which cannot be detected with the standard deviation or other variability measures from time domain. It is interesting to note that the forbidden

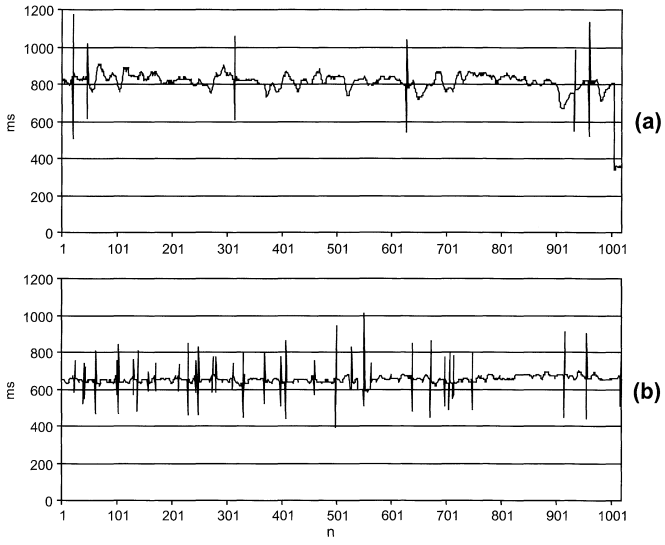

Fig. 6 The last 1000 beat-to-beat intervals before a sustained VT (**a**) and the respective control time series (**b**) from the same patient. To analyse the dynamics just before an arrhythmia, all beat-to-beat intervals of the VT itself at the end of time series (**a**) are removed from the tachograms

Abb. 6 Die letzten 1000 RR-Intervalle vor einer anhaltenden VT (**a**) und die zugehörige Kontrollzeitreihe (**b**) desselben Patienten. Um die Dynamik kurz vor der Arrhythmie zu bestimmen, wurden alle RR-Intervalle der VT selber am Ende der Zeitreihe (**a**) gelöscht

Table 2 Results of finite-time growth rates and of parameters from symbolic dynamics in discriminating the control and VT/VF series

Tab. 2 Ergebnisse der ‚finite-time' Wachstumsraten und der Parameter der symbolischen Dynamik bei der Trennung von Kontroll- und VT/VF-Zeitreihen

	VT/VF	Control	p
$\lambda^{(3,1,1)}$	0.37 ± 0.31	0.51 ± 0.36	n.s.
$\lambda^{(6,1,1)}$	0.22 ± 0.08	0.26 ± 0.05	< 0.05
$\lambda^{(9,1,1)}$	0.11 ± 0.03	0.13 ± 0.02	< 0.05
Forbidden words	32.26 ± 10.50	32.16 ± 9.30	n.s.
H_k	2.13 ± 0.59	2.43 ± 0.43	< 0.05
Plvar10	0.12 ± 0.18	0.04 ± 0.05	< 0.05

word statistics fail to distinguish both groups. The finite-time growth rates were calculated for a five-nearest-neighbours approach. The parameter $\lambda^{(3,1,1)}$ denotes the average growth rate with a dimension of 3, lag 1, and evolution time 1; $\lambda^{(6,1,1)}$, $\lambda^{(9,1,1)}$ respectively. For dimension n=3 there were no significant differences, whereas the average growth rates for $n = 6$ and 9 differed significantly in both groups. For evolution times $T = 2,3$ significant differences disappeared for $n = 6$. Interestingly, for all dimensions the growth rates were larger in the group of the control tachograms than in the VT/VF group, indicating an enhanced predictability or less complex dynamics in the VT/VF group. Additionally, we calculated the average growth rates for different delay times $\tau = 2,3$, evolution time $T = 1$, and $n = 3, \ldots, 9$. For $\tau = 2$ we found a significant difference for $n = 6$ ($p = 0.016$). For $\tau = 3$ we only recognised a considerable but non-significant difference for ($p = 0.052$); no further growth rates showed significant differences between both investigated groups.

Dual sequence method in patients with dilated cardiomyopathy

The baroreflex sensitivity (BRS) is an important parameter to classify patients with reduced left ventricular function. This study aimed at investigating the BRS to differentiate between patients with dilated cardiomyopathy (DCM) and healthy persons (controls) as well as to compare the BRS with heart rate and blood pressure variability.

In 27 DCM patients and 27 age and gender matched controls the electrocardiogram, continuous blood pressure, and respiration curves were recorded. The dual sequence method (DSM) includes the analysis of the spontaneous blood pressure fluctuations and the corresponding RR-intervals of heart rate to estimate the bradycardic baroreflex fluctuations as well as the opposite tachycardic fluctuations. We found a reduced number of heart rate and blood pressure fluctuations in DCM patients compared to the controls (DCM: male: 154.4 ± 93.9, female: 93.7 ± 40.5, controls: m: 245.5 ± 112.9, f: 150.6 ± 55.8, $p < 0.05$). The average slope in DCM patients was lower than in controls (DCM: 5.2 ± 1.9, controls: 8.0 ± 5.4, $p < 0.05$).

A correlation analysis was performed to investigate the different HRV, BPV and BRS parameters for linear dependence (21, 60). In general, the average correlation was low between the different parameter sets ($r = 0.22$). However, several highly correlated parameters were calculated between BRS and HRV (time domain, frequency domain, nonlinear dynamic), and between BRS and BPV, respectively (only frequency domain).

Furthermore, the stepwise discriminant function analysis was used to find the optimal combinations of HRV, BPV and BRS parameters to

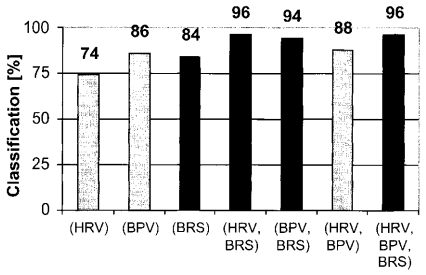

Fig. 7 Results of the discriminant function analysis using different sets of 6 parameters. The black marked bars contain DSM parameters

Abb. 7 Die Ergebnisse der Diskriminanzanalyse unter Verwendung von verschiedenen Sätzen mit je 6 Parametern. Die schwarz markierten Balken enthalten Parameter der dualen Sequenzmethode

differentiate between DCM patients and healthy persons. These combinations of parameters are presented in Fig. 7.

A correct classification of 74–86% was obtained with sets of six parameters from HRV, BPV and BRS. These parameter sets contain mainly three types of information to discriminate between DCM patients and healthy persons: 1) the high frequency in HRV, 2) the mean values and low frequency of BPV and 3) the largest slopes and the number of BR fluctuations.

A set of six parameters from HRV and BPV increased the correct classification up to 88%. Furthermore, the accuracy of classification could be improved using additional BRS parameters. Using a set of six parameters of BPV and BRS a correct classification of 94% was calculated, whereas using a set of six parameters of HRV and BRS the classification accuracy could be improved up to 96%. The use of a six parameters set of HRV, BRV and BRS did not further improve the correct classification greater than 96%.

Optimal transformations for revealing coupling directions

To learn something about the coupling between blood pressure and heart rate, we adopted the view that we do not know anything about the dynamical description of the nonlinear processes that describe the time series of heart rate, x_t, and of blood pressure, y_t, and the coupling between them. In other words, we used the statistical principle of maximum a-priori uncertainty which is the basis of many parameter estimation methods.

However, we need at least a rough model assumption. Since the data are heavily high-pass-filtered to investigate only vagally (respiratory) induced fluctuations, long-range correlations are filtered out and we therefore assume that the system describing the change of heart rate can be written as a map $x_{t+1} = F_1(x_t) + \eta$, where F_1 is an arbitrary function η and some noise. Furthermore, we assume that the variable x is a scalar quantity; all the following considerations can be easily extended to the higher-dimensional case. Since the method, as applied to heart rate and blood pressure works well for the simplest case of scalar state variables, we do not go into detail with respect to this extension. Including the coupling between x and y, the overall system is assumed to be

$$x_{t+1} = F_1(x_t) + F_2(x_t - y_t) + \eta_x \tag{24}$$

$$y_{t+1} = G_1(y_t) + G_2(y_t - x_t) + \eta_y \tag{25}$$

The functions F_2 and G_2 are coupling functions that depend on the difference between the two systems, an assumption that is often met in modelling synchronising systems. Now, using the principle of maximum a-priori uncertainty, the functions F_1, F_2, G_1 and G_2 are estimated from pairs of time series, using the maximal correlation method. We use a modified ACE-algorithm where the function Θ in Eq. (21) is fixed to be the identity function since in the model (24, 25) it is not needed.

For each of the four analysed pairs of heart rate and blood pressure, we find a maximal correlation very close to unity ($\Psi > 0.98$) with the chosen smoothing kernel. This shows that the model can explain most of the variance observed in the data; physiologically speaking there is nearly a one-to-one relationship between respiratory induced variability in blood pressure and in heart rate. The results for the four analysed pairs of time series are depicted in Fig. 8.

The functions F_1, and G_1, describing the dynamics of the uncoupled systems, are close to linear and are not shown. The coupling functions $F_2(x_t - y_t)$, however, show a strong nonlinear behaviour whereas the functions $G_2(y_t - x_t)$ are nearly flat. This is a strong indication that, assuming the crude assumption of Eqs. (24, 25) which should be in first order a good approximation to the observed dynamics, the heart rate is strongly influenced by the blood pressure but not vice versa. Therefore, the total system is highly skewed, or, in other words, a drive-response system where blood pressure is the driver and heartbeat the response. This is in agreement with the widely accepted explanation for respiratory sinus arrhythmia in heart rate, which mostly reflects arterial baroreflex buffering of respiration-induced arterial pressure fluctuations (56).

Discussion

We have introduced different nonlinear approaches to heart rate and blood pressure variability analysis and their application to different clinical studies.

Symbolic dynamics is a useful tool in several fields of complexity analysis in science. We have applied symbolic dynamics mainly to characterise the dynamics of heart rate variability. Symbols represent levels of time differences between succes-

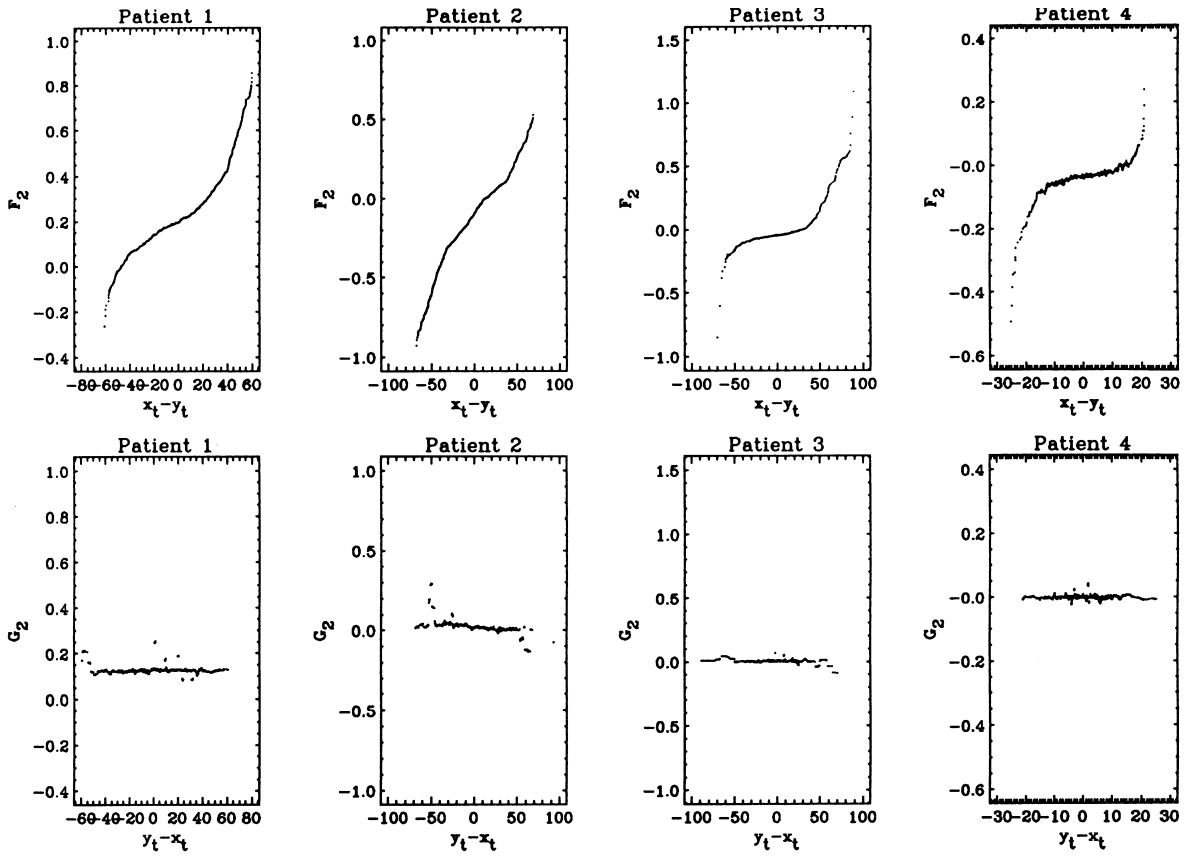

Fig. 8 Top row: For the four analysed data sets the estimated coupling function $F_2(x_t - y_t)$ from Eq. (24), describing the influence of blood pressure on heart rate. Bottom row: The same for the other coupling direction, i.e., the function $G_2(y_t - x_t)$ from Eq. (25), describing the influence of heart rate on blood pressure. For a better comparison, the plots in each column, corresponding to the same data set, are normalised so that a quantitative comparison of the two plots in each column can be performed. One notices that in the bottom row the coupling functions are almost completely flat; it seems to be that there is no influence of heart rate on blood pressure

Abb. 8 Obere Reihe: Für die vier analysierten Datensätze sind die geschätzten Kopplungsfunktionen $F_2(x_t - y_t)$ aus Formel (24) dargestellt, sie beschreiben den Einfluss des Blutdrucks auf die Herzfrequenz. Untere Reihe: Dieselbe Darstellung für die andere Kopplungsrichtung, d.h. die Funktion $G_2(y_t - x_t)$ aus Gl. (25), welche den Einfluss der Herzfrequenz auf den Blutdruck darstellen. Damit man die Ergebnisse besser vergleichen kann, sind die Grafiken welche zu einer Person gehören normiert. Aus den Grafiken ist zu ersehen, dass die unteren Kopplungsfunktionen alle nahezu flach sind, das bedeutet, dass es wenig Einfluss der Herzfequenz auf den Blutdruck zu geben scheint

sive beats. We showed that symbolic dynamics is an independent method (low correlations to standard time and frequency measures) and increases the predictive accuracy in high risk stratification. Complexity measures based on nonlinear dynamics separate best between different patient groups because of the partly nonlinear behaviour of the heart rate generation. The combination of parameters of time and frequency domain and nonlinear dynamics leads to an optimal detection rate of patients after myocardial infarction with high risk for sudden cardiac death. Moreover, symbolic dynamics is a method with a very close connection to physiological phenomena and is relatively easy to interpret.

The renormalised entropy method RE_{AR} is designed in such a way that tachograms with normal variability and typical periodograms have negative values of RE_{AR}. Either a decreased HRV (under stress or even at rest) or pathological spectra lead to positive values of RE_{AR}. Pathological spectra are periodograms with dominant ULF, VLF or LF peaks. Dominant ULF or VLF peaks are seen in tachograms without any respiratory modulations and without any influence of blood pressure regulation. Dominant LF peaks are recognisable in tachograms without any long-term regulation and decreased vagal activity. The results of the St. George's hospital postinfarction data base study (66) (not shown here) confirmed the hypothesis that the survivors on average have negative and the deceased positive values of renormalised entropy. Calculating renormalised entropy assumes a fixed reference distribution. In this study the reference distribution was

selected using the interchanging algorithm applied to the data of 23 healthy persons. In future HRV studies, it needs to be investigated if a general or a disease dependent reference distribution should be chosen.

The aim of the forecasting study was to find heart rate variability changes just before the onset of ventricular tachycardia or ventricular fibrillation (VT/VF), i.e., to look for some precursor-like activities before this qualitative change. Two approaches from nonlinear dynamics indeed exhibit significant changes in heart rate variability: methods of symbolic dynamics and finite-time growth rates. It is important to note that standard linear techniques are not able to discriminate between these both groups. From finite-time growth rates we obtain significant differences between the VT/VF and the control time series only for relatively high dimension ($n > 5$). This indicates that the changes are mainly caused by sympathetic activities of the autonomous nervous system. Vagal activities would affect smaller dimensions. These results are in good agreement with the physiological fact that the sympathetic activity increases before the onset of VT. The significantly lower values of the finite-time growth rates in the VT/VF group provide a possibility to predict a VT/VF. The calculation with different delays τ for the embedding has shown the importance of analysing beat-to-beat variability; no successive heart beats should be removed. For delays greater than one, significant differences in the average growth rates decreased, which shows that the differences between the VT/VF time series and the controls are caused by beat-to-beat regulation. Moreover, this study demonstrated the advantage of using methods from nonlinear dynamics. The evolution of points in phase space provides deeper insight into dynamical aspects of the cardiac system. Limitations of this study are the relatively small number of time series and the reduced statistical analysis (no subdivisions concerning age, sex, and heart disease). For this reason, these results have to be validated on a larger data base.

The analysis of the baroreflex sensitivity (BRS) is an established method for improved classification of different cardiac diseases. In contrast to standard BRS methods, the dual sequence method (DSM) considers shifted bradycardic and tachycardic fluctuations. The biosignals of patients are recorded at rest and without any additional challenge (e.g. application of drugs and other stimuli). The analysis showed that there are significant differences between DCM patients and healthy persons with respect to the calculated parameters. In DCM patients and healthy persons we calculated the mean values of heart rate and blood pressure to determine the difference in the active range of the blood pressure. The determination of the active range of the blood pressure, the value of the average RR-interval of DCM patients, was calculated to be 795.9 ± 107.7 ms. This value is considerably lower than in the control group (862.4 ± 130.5 ms, $p < 0.05$). The values of the average blood pressure in DCM patients and in healthy persons behave inversely to the heart rate values (DCM: 101.5 ± 19.6 mmHg, Controls: 112.9 ± 25.7 mmHg, $p < 0.05$). Hence we can see that the autonomous regulation in DCM patients seems to be more ineffective than in healthy persons. This behaviour is characterised by the lower number of the baroreflex fluctuations and by the lower average slope of BRS. In comparison to the standard sequence method, the DSM obtained an improved accuracy of classification (84% versus 76%). The consideration of DSM parameters in combination with HRV and BPV parameters leads to a significant increase of discriminant power (96%). Summarising, the dual sequence method increases the information about the cardiovascular system.

Revealing the coupling direction and the strength of coupling via optimal transformations is a new and promising approach. No a priori assumptions about the dynamical system that regulates heart rate and blood pressure has to be made. In this contribution first the respiratory induced fluctuations were investigated and long-range correlations were filtered out. The results of the four bivariate data sets analysed here strongly indicate and confirm the knowledge of respiratory sinus arrhythmia in heart rate: it reflects baroreflex buffering of respiration-induced arterial pressure fluctuations. In Taylor et al. (56) it was also shown that there is an influence of heart rate on blood pressure variability. Therefore, we next have to investigate the influence of high-pass filtering to coupling directions. However, the approach introduced here seems to be useful for determining nonlinear coupling between heart rate and blood pressure. Moreover, on a larger data base the coupling directions have to be investigated more intensively.

In conclusion, this paper demonstrated that parameters from nonlinear dynamics are meaningful for risk stratification after myocardial infarction, for the prediction of VT/VF events even in short-term HRV time series and for modelling the relationship between heart rate and blood pressure variability. These findings seem to be of importance for clinical diagnostics, in algorithms for risk stratification and to improve the therapeutic and preventive tools of next generation ICDs.

References

1. Abarbanel HDI, Brown R, Kennel MB (1991) Lyapunov exponents in chaotic systems: their importance and their evaluation using observed data. Int J Mod Phys B 5:1347–1375
2. Almog Y, Eliash S, Oz O, Akselrod S (1996) Nonlinear analysis of BP signal: can it detect malfunctions in BP control? Am J Physiol Heart Circulatory Physiol 40:H396-H403
3. Babloyantz A, Destexhe A (1988) Is the normal heart a periodic oscillator? Biol Cybern 58:203–211
4. Barron HV, Lesh MD (1996) Autonomic nervous system and sudden cardiac death. J Am Coll Cardiol 27(5):1053–1060
5. Berntson GG, Quigley KS, Jang JF, Boysen ST (1990) An approach to artifact identification: application to heart period data. Psychophysiology 27:586–598
6. Bertinieri G, di Rienzo M, Cavallazzi A, Ferrari AU, Pedotti A, Mancia G (1988) Evaluation of baroreceptor reflex by blood minitoring in unanesthezed cats. Am J Physiol 254:H377–H383
7. Bettermann H, Amponsah D, Cysarz D, van Leeuwen P (1999) Musical rhythms in heart period dynamics: a cross-cultural and interdisciplinary approach to cardiac rhythms. Am J Physiol 277(5 Pt 2):H1762–1770
8. Braun C, Kowallik P, Freking A, Hadeler D, Kniffki KD, Meesmann M (1998) Demonstration of nonlinear components in heart rate variability of healthy persons. Am J Physiol 275(5 Pt 2):H1577–1584
9. Breiman L, Friedman JH (1985) Estimating optimal transformations for multiple regression and correlation. J Am Stat Assoc 80:580–619
10. Brown R, Bryant P, Abarbanel HDI (1991) Computing the Lyapunov spectrum of a dynamical system from an observed time series. Physical Review A 43:2787–2806
11. Damiano RJ Jr (1992) Implantable cardioverter defibrillators: current status and future directions. J Card Surg 7(1):36–57
12. Ducher M, Fauvel JP, Gustin MP, Cerutti C, Najem R, Cuisinaud G, Laville M, Pozet N, Paultre CZ (1995) A new noninvasive statistical method to assess the spontaneous cardiac baroreflex in subjects. Clinical Science 88:651–655
13. Eckmann JP, Oliffson Kamphorst S, Ruelle D, Ciliberto S (1986) Lyapunov exponents from time series. Physical Review A 34:4971–4879
14. Engbert R; Schiek M, Scheffczyk C, Kurths J, Krampe R, Kliegl R, Drepper F (1997) Symbolic dynamics of physiological synchronization: examples from bimanual movements and cardiorespiratory interaction. Nonlinear Analysis Theory Methods And Applications 30(2):973–984
15. Fei L, Anderson MH, Statters DJ, Malik M, Camm AJ (1995) Effects of passive tilt and submaximal exercise on spectral heart rate variability in ventricular fibrillation patients without significant structural heart disease. Am Heart J 129(2): 285–290
16. Gebelein H (1941) Das statistische Problem der Korrelation als Variations- und Eigenwertproblem und sein Zusammenhang mit der Ausgleichsrechnung. Z angew Math Mech 21:364–379
17. Glass L, Mackey MC (1988) Noise and Chaos. In: Anonymous (ed) From Clocks to Chaos. Princeton University Press, Princeton, pp 1–241
18. Goldberger AL, Findley LJ, Blackburn MR, Mandell AJ (1984) Nonlinear dynamics in heart failure: implications of long-wavelength cardiopulmonary oscillations. Am Heart J 197:612–615
19. Haaksma J, Dijk WA, Brouwer J, van den Berg MP, Crijns HJGM, Lie KI (1995) Effects of automatic ectopy exclusion on the analysis of heart rate variability using a percentile exclusion rule. Computers in Cardiology, Los Alamitos, IEEE Society Press, pp 197–200
20. Hadamard J (1898) Les surfaces à courbures opposées et leurs lignes geodésiques. J Math Pures Appl 27–73
21. Heart rate variability: standards of measurement, physiological interpretation and clinical use. Task Force of the European Society of Cardiology and the North American Society of Pacing and Electrophysiology (1996) Circulation 93(5):1043–1065
22. Hirschfeld HO (1935) A connection between correlation and contingency. Proc of the Camb Phil Soc 31:520–524
23. Hoyer D, Hoyer O, Zwiener U (2000) A new approach to uncover dynamic phase coordination and synchronization. IEEE Trans Biomed Eng 47(1):68–74
24. Hoyer D, Kaplan D, Schaaff F, Eiselt M (1998) Determinism in bivariate cardiorespiratory phase-space sets. IEEE Eng Med Biol Mag 17(6):26–31
25. Janse MJ (1995) Chaos in the prediction of sudden death. Eur Heart J 16:299–301
26. Kleiger RE, Miller JP, Bigger JT, Moss A (1987) Decreased heart rate variability and its association with increased mortality after acute myocardial infarction. Am J Cardiol 59:256–262
27. Kobayashi M, Musha T (1982) 1/f fluctuation of heartbeat period. IEEE Trans on Biomed Eng 29:456–457
28. Kopitzki K, Warnke PC, Timmer J (1998) Quantitative analysis by renormalized entropy of invasive electroencephalograph recordings in focal epilepsy. Physical Review E 58:4859–4864
29. Kurths J, Herzel H (1987) An attractor in a solar time series. Physica D 25: 165–172
30. Kurths J, Voss A, Witt A, Saparin P, Kleiner HJ, Wessel N (1995) Quantitative analysis of heart rate variability. Chaos 5:88–94
31. Lippman N, Stein KM, Lerman BB (1994) Comparison of methods for removal of ectopy in measurement of heart rate variability. Am J Physiol 267(1 Pt 2):H411-418
32. Lombardi F (2000) Chaos theory, heart rate variability, and arrhythmic mortality. Circulation 101(1):8–10
33. Lombardi F, Sandrone G, Mortara A, Torzillo D, La Rovere MT, Signorini MG, Cerutti S, Malliani A (1996) Linear and nonlinear dynamics of heart rate variability after acute myocardial infarction with normal and reduced left ventricular ejection fraction. Am J Cardiol 77: 1283–1288
34. Lorenz EN (1965) A study of the predictability of a 28-variable atmospheric model. Tellus 17:321–333
35. Makikallio TH, Hoiber S, Kober L, Torp-Pedersen C, Peng CK, Goldberger AL, Huikuri HV (1999) Fractal analysis of heart rate dynamics as a predictor of mortality in patients with depressed left ventricular function after acute myocardial infarction. TRACE Investigators. TRAndolapril Cardiac Evaluation. Am J Cardiol 83(6):836–839
36. Malberg H (1999) Modellierung, Analyse und Klassifikation von autonomen Regulationsprozessen des Herz-Kreislauf-Systems, Dissertation, University Ilmenau, Fortschr.-Ber. VDI Reihe 2000, 17(192), VDI Verlag Düsseldorf
37. Malberg H, Wessel N, Schirdewan A, Osterziel KJ, Voss A (1999) Duale Sequenzmethode zur Analyse der spontanen Baroreflexsensitivität bei Patienten mit dilatativer Kardiomyopathie. Z Kardiol (88)5:331–337
38. Mancia G, Grassi G, Bertinieri G, Ferrari A, Zanchetti A (1984) Arterial baroreflex control of blood pressure in man. J Auton Nerv Syst 11:115–124
39. Mancia G, Grassi G, Ferrari A, Zanchetti A (1985) Reflex cardiovascular regulation in human. J Cardiovasc Pharmacol 7 (Suppl. 3):152–159
40. Morse M, Hedlund GA (1938) Symbolic dynamics. American J Math 60:815–866

41. Morse M (1921) Recurrent geodesics on a surface of negative curvature. Trans Amer Math Soc 22:84–110
42. Nese JM (1989) Quantifying local predictibility in phase space. Physica D 35:237–250
43. Oseledec VI (1968) A multiplicative ergodic theorem, Ljapunov characteristic numbers for dynamical systems. Transactions of the Moscow Mathematical Society 19:197–231
44. Palazzolo JA, Estafanous FG, Murray PA (1998) Entropy measures of heart rate variation in conscious dogs. Am J Physiol Heart Circul Physiol 43(4):H1099–H1105
45. Parati G, DiRienzo M, Bertinieri G, Pomidossi G, Casadei R, Gropelli A, Pedotti A, Zanchetti A, Mancia G (1988) Evaluation of the baroreceptor-heart rate reflex by 24-hour intra arterial blood pressure monitoring in humans. Hypertension 12(2):214–222
46. Parlow J, Viale JP, Annat G, Hughson R, Quintin L (1995) Spontaneous cardiac baroreflex in subjects. Comparison with drug-induced responses. Hypertension 25:1058–1068
47. Paulus MP, Geyer MA, Gold LH, Mandell AJ (1990) Application of entropy measures derived from the ergodic theory of dynamical systems to rat locomotor behavior. Proc Natl Acad Sci USA 87(2):723–727
48. Rapp PE, Schmah T (1996) Complexity measures in molecular psychiatry. Molec Psychiatry 1(5):408–416
49. Rényi (1970) Probability Theory. Akadémiai Kiadó, Budapest
50. Rosenblum MG, Pikovsky AS, Kurths J (1996) Phase synchronization of chaotic oscillators. Physical Review Letters 76: 1804–1807
51. Saparin P, Witt A, Kurths J, Anishenko V (1994) The renormalized entropy- an appropriate complexity measure. Chaos, Solitons and Fractals 4(10):1907–1916
52. Schäfer C, Rosenblum MG, Kurths J, Abel HH (1998) Heartbeat synchronized with ventilation. Nature 392(6673):239–240
53. Smith LA (1994) Local optimal prediction: exploiting strangeness and the variation of sensitiy to initial condition. Phil Trans R Soc Lond A 348(1688):371–381
54. Takens F (1981) Detecting strange attractors in turbulence. In: Rand E, Young LS (eds) Dynamical Systems and Turbulence, Warwick. Lecture Notes in Mathematics 898. Springer, Berlin, 1981, pp 366–381
55. Tass P, Rosenblum MG, Weule J, Kurths J, Pikovsky AS, Volkmann J, Schnitzler A, Freund HJ (1998) Detection of n : m phase locking from noisy data: application to magnetoencephalography. Physical Review Letters 81:3291–3294
56. Taylor JA, Eckberg DL (1996) Fundamental relations between short-term RR interval and arterial pressure oscillations in humans. Circulation 93(8):1527–1532
57. Tsuji H, Larson MG, Venditti FJ Jr, Manders ES, Evans JC, Feldman CL, Levy D (1996) Impact of reduced heart rate variability on risk for cardiac events. The Framingham Heart Study. Circulation 94(11):2850–2855
58. Voss A, Hnatkova K, Wessel N, Dietz R, Malik M (1997) Non-Linear Parameters Contribute to Heart Rate Variability Analysis Independently from Time and Frequency Measures. Proceedings of Europace. Monduzzi Editore, pp 191–195
59. Voss A, Hnatkova K, Wessel N, Kurths J, Sander A, Schirdewan A, Camm AJ, Malik M (1998) Multiparametric analysis of heart rate variability used for risk stratification among survivors of acute myocardial infarction. Pacing Clin Electrophysiol 21(1Pt2):186–192
60. Voss A, Kurths J, Kleiner HJ, Witt A, Wessel N, Saparin P, Osterziel KJ, Schurath R, Dietz R (1996) The application of methods of non-linear dynamics for the improved and predictive recognition of patients threatened by sudden cardiac death. Cardiovasc Res 31:419–433
61. Voss H, Kurths J (1997) Reconstruction of nonlinear time delay models from data by the use of optimal transformations. Physics Letters A 234:336–344
62. Voss H, Kurths J (1999) Reconstruction of nonlinear time delay models from optical data. Chaos, Solitons and Fractals 10:805-809
63. Voss HU, Kolodner P, Abel M, Kurths J (1999) Amplitude equations from spatiotemporal binary-fluid convection data. Phys Rev Lett 83:3422–3425
64. Voss HU, Schwache A, Kurths J, Mitschke F (1999) Equations of motion from chaotic data: a driven optical fiber ring resonator. Physics Letters A 256:47–54
65. Wackerbauer R, Witt A, Atmanspacher H, Kurths J, Scheingraber H (1994) A comparative classification of complexity measures. Chaos Solitons Fractals 4:133–173
66. Wessel N (1998) Komplexe Analyse nichtlinearer Phänomene in kardiologischen Datenreihen. Dissertation. University of Potsdam
67. Wessel N, Voss A, Kurths J, Saparin P, Witt A, Kleiner HJ, Dietz R (1994) Renormalised entropy: a new method of nonlinear dynamics for the analysis of heart rate variability. Los Alamitos: Computers in Cardiology. IEEE Computer Society Press, pp 137–140
68. Wessel N, Ziehmann Ch, Kurths J, Meyerfeldt U, Schirdewan A, Voss A (2000) Short-term forecasting of life-threatening cardiac arrhythmias based on symbolic dynamics and finite-time growth rates. Phys Rev E 61(1):733–739
69. Wolf A, Swift JB, Swinney HL, Vastano JA (1985) Determining Lyapunov Exponents from a time series. Physica D 16:285–317
70. Xu JH, Liu ZR, Liu R (1994) The measures of sequence complexity for EEG studies. Chaos 4(11):2111–2119
71. Yoden S, Nomura M (1993) Finite-time lyapunov stability analysis and its application to atmospheric predictability. Journal of the Atmospheric Sciences 50: 1531–1543
72. Zebrowski JJ, Poplawska W, Baranowski R, Buchner T (1995) Local time properties of 24-hour holter recordings of RR intervals: a nonlinear quantitative method trough pattern entropy of 3-D return maps. Computers in Cardiology. IEEE Society Press. Los Alamitos, pp 377–380
73. Ziehmann C, Smith LA, Kurths J (1999) The bootstrap and Lyapunov exponents in deterministic chaos. Physica D 126: 49–59